

Location-Assisted Graph-Based User Scheduling in Multi-User MIMO LEO NTN Systems

Original

Location-Assisted Graph-Based User Scheduling in Multi-User MIMO LEO NTN Systems / Ahmad, B.; Riviello, D.; Defilippo, B.; Guidotti, A.; Vanelli-Coralli, A.. - In: INTERNATIONAL JOURNAL OF SATELLITE COMMUNICATIONS AND NETWORKING. - ISSN 1542-0973. - ELETTRONICO. - (2025), pp. 1-13. [10.1002/sat.70006]

Availability:

This version is available at: 11583/3004432 since: 2025-10-24T11:16:05Z

Publisher:

Wiley

Published

DOI:10.1002/sat.70006

Terms of use:

This article is made available under terms and conditions as specified in the corresponding bibliographic description in the repository

Publisher copyright

(Article begins on next page)

SPECIAL ISSUE PAPER OPEN ACCESS

Location-Assisted Graph-Based User Scheduling in Multi-User MIMO LEO NTN Systems

Bilal Ahmad¹  | Daniel Gaetano Riviello²  | Bruno De Filippo¹  | Alessandro Guidotti³  | Alessandro Vanelli-Coralli¹ 

¹Department of Electrical, Electronic, and Information Engineering, University of Bologna, Bologna, Italy | ²CNR-IEIIT, Istituto di Elettronica e Ingegneria dell'Informazione e delle Telecomunicazioni, Consiglio Nazionale delle Ricerche, Torino, Italy | ³National Inter-University Consortium for Telecommunications (CNIT), University of Bologna Research Unit, Bologna, Italy

Correspondence: Daniel Gaetano Riviello (daniel.riviello@cnr.it)

Received: 22 April 2024 | **Revised:** 29 November 2024 | **Accepted:** 4 August 2025

Funding: This work was partially supported by the European Union under the Italian National Recovery and Resilience Plan (NRRP) of NextGenerationEU, partnership of "Telecommunications of the Future" (PE00000001- program "RESTART"), and funded by the 6G-NTN project, which received funding from the Smart Networks and Services Joint Undertaking (SNS JU) under the European Union's Horizon Europe Research and Innovation Programme under grant agreement no. 101096479. The work of Daniel Gaetano Riviello was partially supported by the European Union - NextGenerationEU - National Recovery and Resilience Plan (Piano Nazionale di Ripresa e Resilienza, PNRR) through the Project: "SoBigData.it - Strengthening the Italian RI for Social Mining and Big Data Analytics", under grant prot. IR0000013 - Avviso no. 3264 del 28/12/2021.

Keywords: beamforming | maximum clique | MIMO | NTN | user scheduling

ABSTRACT

This paper addresses user clustering and scheduling for multi-user MIMO low Earth orbit nonterrestrial network systems in full frequency reuse. Since the number of on-ground user terminals is usually much higher than the number of on-board LEO satellite antennas, user scheduling becomes a fundamental task. We accomplish user scheduling by grouping users into clusters. Users within the same cluster are served by the satellite at the same time by means of space division multiplexing via location-based feed space digital beamforming. Each cluster is then assigned to a distinct time slot and served by means of time division multiplexing. Given the full frequency reuse nature of the system, we design user scheduling algorithms with the goal of maximizing the average per-user throughput while minimizing the co-channel interference and preserving fairness among users. To this aim, we propose in this paper (a) a distance-based iterative graph-based scheduler based on the maximum clique approach and (b) a distance-based implementation of the multiple antenna downlink orthogonal user clustering algorithm. For both these schedulers, the great circle distance between the users is employed as a dissimilarity metric to compute the user adjacency matrix, avoiding the need for the transmission of downlink pilots for channel state information estimation. To further validate our analysis, the proposed approaches are compared with (a) channel state information-based graph and maximum clique approach and (b) original multiple antenna downlink orthogonal user clustering algorithm. Extensive simulations assess the achievable per-user throughput and signal-to-noise plus interference ratio achieved by the proposed schedulers, highlighting the impact that the distance-based metric has on the system performance. This study provides valuable insights into the effective use of user scheduling algorithms.

This is an open access article under the terms of the [Creative Commons Attribution](https://creativecommons.org/licenses/by/4.0/) License, which permits use, distribution and reproduction in any medium, provided the original work is properly cited.

© 2025 The Author(s). *International Journal of Satellite Communications and Networking* published by John Wiley & Sons Ltd.

1 | Introduction

Nonterrestrial network (NTN) systems are expected to have a significant impact on the future advancement of wireless networks. Thanks to their inherent attributes, they represent a key enabler to achieve the ambitious objective of providing services everywhere, at any time, and on any device. Specifically, NTN systems are instrumental in extending and complementing terrestrial coverage in unserved and underserved areas, as well as in providing connectivity to vertical markets [1].

The upcoming generations of wireless networks are expected to connect an extremely large number of devices with fast data transfer rates and minimal latency. To this aim, low earth orbit (LEO) satellites are considered a promising technology to revolutionize several beyond fifth-generation (B5G) and sixth-generation (6G) application cases [2]. When compared with Geostationary orbit (GEO) satellites, LEO satellites possess several advantages, for example, lower power consumption and reduced propagation latency requirements [3].

However, one of the major challenges of NTN is to provide significant capacity to support service requirements while managing the limited available frequency spectrum [4]. To this aim, NTN focuses on full frequency reuse (FFR) approaches that on one side maximize the exploitation of the available spectrum and on the other side introduce significant interference that shall be dealt with by the system. To improve the transmission data rates, the recent trend is to adopt the multibeam (MB) architectures to obtain higher power flux density per beam and increase the spectrum's reuse factors.

Multiple-input-multiple-output (MIMO) is one of the key enablers of MB satellites, improving their data rate and boosting their spectral efficiency. LEO satellites equipped with antenna arrays can efficiently deliver services to many user terminals (UTs) through the implementation of digital beamforming algorithms in the feed space (FS) [5]. Under this framework, transmissions in areas characterized by high UT density may lead to a substantial amount of interference and, as a result, a notable reduction in the per-user throughput. To address this issue, user scheduling algorithms have to be employed to ensure adequate performance while also maintaining good fairness levels among the users. Due to the complexity of the problem, the design of scheduling algorithms can be challenging. To improve the sum-rate capacity of the NTN system, one possibility is to exploit clustering algorithms to avoid scheduling users with similar channel conditions, which may lead to the scheduled channel matrix to be rank deficient. Users within the same cluster, or group, are subsequently served collectively using space division multiplexing (SDM) through digital beamforming methods, with each group being scheduled to separate time intervals using time division multiplexing (TDM) [6]. Clearly, several decision criteria may be employed to define user clusters. The majority of user grouping algorithms employs the channel coefficient of correlation (CoC) metric due to its capability to measure the spatial compatibility between two users. This metric takes into account both orthogonality and individual channel gains, thus making it a dependable indicator for scheduling one user without

impacting the other users at the expense of obtaining variable-sized clusters [7].

The process of identifying the optimal subset of UTs for scheduling is an intricate optimization problem referred to be non-deterministic polynomial-time (NP)-complete [4]. Consequently, there is a prevailing tendency to create suboptimal solutions that find a compromise between computational complexity and performance.

1.1 | Previous Works

A substantial amount of literature has been produced on user scheduling and beamforming design in satellite communication (SATCOM) systems. Two different scheduling approaches can be distinguished in literature: (i) scheduling and clustering for multicast transmission, in which the objective is to group users based on a similarity measure (e.g., similar channel), and adopt the same precoder for the whole group and (ii) scheduling and clustering for unicast transmission, in which the objective is to group users based on a dissimilarity measure, that is, serve users in the same group through SDM and separate each group through TDM. The scheduling approaches for multicast transmission mainly focus on GEO and use clustering techniques based on centroid or connectivity models (i.e., k-means). In [8], the authors adopt a scheduling approach with joint multicast precoding based on spectral clustering, in which they construct a graph with similarity matrix based on the Euclidean distance between users' channel vectors, and they apply the k-means algorithm on the eigenvectors associated with the lowest eigenvalues of the Laplacian matrix associated to the graph. In [9], the authors examine precoding design in a MB-SATCOM system to maximize the throughput. This research focuses on achieving optimal user scheduling and beamforming, taking into account the availability of perfect channel state information (CSI). The study conducted in [10] examines a resilient multigroup multicast transmission scheme for a MB-SATCOM system and presents a beamforming algorithm with low complexity, along with a user grouping algorithm. The study further examines the influence of CSI errors on the optimization objective of power minimization. The authors of [11] examined the design of the multigroup multicast transmission scheme in frame-based MB SATCOM systems. This work proposes a joint design scheme for user scheduling and beamforming which relies on accurate CSI. The main goal of this scheme is to maximize spectrum efficiency. In [6], the design of joint scheduling and precoding techniques is presented for multi-user multiple-input single-output (MU-MISO) downlink (DL) channels with perfect CSI. The overall problem of selecting users for multicast precoding has been regarded as a clustering problem. This study further yields qualitative outcomes in the context of maximizing the overall sum-rate. The authors of [12] proposed an equivalent distance metric for scheduling, incorporating the experienced interference level, the slant range, and the number of antenna elements on board of the satellite. The scheduler computes the metric in an iterative fashion, aiming at approximating the signal-to-interference-plus-noise ratio (SINR) of each user.

With regard to scheduling and clustering for unicast transmission, within the existing literature, the challenge of user

scheduling is approached in two distinct ways: (a) *SINR-based scheduling* and (b) *non-SINR-based scheduling*. The first approach involves the initial computation of the SINR for each user. Afterwards, the user u is allocated to the group that has the least effect on the resulting SINR. Nevertheless, this approach becomes unfeasible when managing a large number of users per spot beam within a reasonable time frame. An exemplary algorithm in this classification is the State-of-the-Art (SOA) sum rate maximization user grouping (SMUG) algorithm [13], which demonstrates exceptional performance when the overall number of users in the system is relatively small. The SMUG algorithm employs a systematic approach to choose users from a pool of potential candidates, taking into account the overall number of available time slots. The goal is to maximize the current sum-rate while guaranteeing a consistent increase in the sum-rate for each subsequent time slot. Differently, the non-SINR-based approaches evaluate the spatial suitability of two users in a MU-MIMO system using a computationally efficient measure, that is, the CoC. Further details on this methodology can be found in [7]. The multiple antenna downlink orthogonal clustering (MADOC) algorithm is a renowned SOA scheduler that uses a non-SINR-based approach [14].

1.2 | Contribution and Notation

This paper is an extended version of our work in [15] and presents a new radio resource management (RRM) method based on the system model from our prior works [15–18]. While our prior research primarily concentrated on the S-band, this extension significantly enhances RRM research within the Ka-band frequency range. The key contributions of this paper are as follows:

- We formulate a novel grouping indicator and ensured its compatibility with two CSI-based SOA schedulers, namely, the original MADOC algorithm [14], and the graph-based iterative maximum clique scheduler (IMCS) [16]. This indicator does not necessitate the use of CSI during the scheduling phase; rather, it solely relies on the geographic positions of users, reducing the amount of overhead required by the SATCOM system. The main goal is to improve the total sum-rate capacity of the system while also guaranteeing fairness among users.
- To validate our improvements, we conduct a comprehensive comparative analysis between the two CSI-based schedulers (named C-MADOC and C-IMCS) and their newly proposed distance-based counterparts (D-MADOC and D-IMCS). The purpose of this comparative analysis is to assess the effectiveness and advantages of the distance-based algorithms and to further provide a comprehensive understanding of how the use of location-based grouping indicators can affect the performance and efficiency of schedulers.
- We consider a full location-based framework, in which not only the scheduling algorithms are distance-based but also beamforming is location-based; that is, we implement SDM within each group via FS Location-based minimum mean square error (LB-MMSE), in which the users' channel vectors are inferred from their position.

We report in Table 1 the terminology and notation used throughout the paper, along with their description.

2 | System Model

The system model has been adapted from our previous studies [15–18] to maintain consistency. A standalone LEO satellite equipped with a uniform planar antenna array (UPA) is considered. The antenna array is composed of N radiating elements, providing connectivity to K uniformly distributed on-ground users. While the growing SatCom user base may let the user distribution deviate to being nonuniform [19], we here consider only stationary UTs in rural areas with low user density; thus, the traditional uniformity assumption is reasonable. In this setup, the serving ground node base station (gNB), which is assumed to be situated on the ground and within the satellite's visibility, is responsible for scheduling multiple data transmissions in each scheduling frame. It serves users through SDM using FS location-based digital beamforming techniques. Typically, to execute these tasks, the gNB transmits pilot signals at the initial time τ_0 , enabling users to estimate their DL CSI, which is then relayed back to the gNB to determine the optimal user scheduling. However, this process introduces overhead that diminishes the system's overall throughput. Therefore, as illustrated in Figure 1, in each scheduling window, we propose that a global navigation satellite system (GNSS)-enabled UT k communicates its

TABLE 1 | Adopted terminology and notation.

\mathbf{A}^T	Transpose of matrix \mathbf{A}
\mathbf{A}^H	Conjugate transpose of matrix \mathbf{A}
$\text{diag}(\mathbf{A})$	Vector containing diagonal elements of \mathbf{A}
$\text{diag}(\mathbf{a})$	Diagonal matrix constructed from vector \mathbf{a}
$[\mathbf{A}]_{ij}$	Element at row i and column j of matrix \mathbf{A}
N_H, N_V	No. of array elements in y - and z -axes
$N = N_H \cdot N_V$	Total no. of array elements
d_H, d_V	Inter-element distance on y - and z -axes
κ	Boltzmann constant
B	User bandwidth
$T_k = T$	Equivalent noise temperature of UT k
d_k	Slant range of UT k
λ	Carrier wavelength
$k_0 = 2\pi\lambda$	Wave number
$g_E(\theta, \varphi)$	Radiation pattern of antenna elements
$G_k^{(rx)}$	Reception antenna gain for UT k
\mathbf{I}_K	$K \times K$ identity matrix
P_t	Total onboard power
P_n	Noise power
L_k	Additional propagation losses for UT k

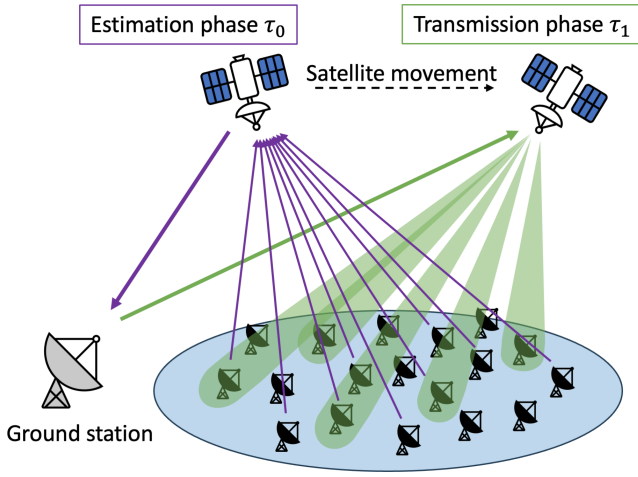


FIGURE 1 | LEO NTN system architecture.

estimated position at time τ_0 to the gNB instead of sending DL CSI, thereby removing the necessity for dedicated DL pilots for scheduling. These positional data are processed by the RRM functions, culminating in the satellite transmitting the scheduled symbols at time $\tau_1 = \tau_0 + \Delta\tau$. It is evident that the delay $\Delta\tau$ between position estimation and DL transmission impacts system performance, as the aging of the channel due to satellite and potentially user movement can lead to suboptimal scheduling and beamforming matrix calculations for the actual transmission channel. This latency comprises the maximum propagation delay on the uplink user link within the coverage area ($\tau_{UT,max}$), the DL and uplink propagation delays on the feeder link (both assumed to be equal to τ_{feeder}), processing delays from RRM (τ_p), and additional system delays (τ_{ad}). The total latency $\Delta\tau$ can be then expressed as follows:

$$\Delta\tau = \tau_{UT,max} + 2\tau_{feeder} + \tau_p + \tau_{ad} \quad (1)$$

where $\tau_{UT,max}$ denotes the maximum propagation delay for a UT in the satellite's coverage area while requesting connectivity, τ_{feeder} represents feeder link propagation latency, τ_p is the beamforming matrix computation processing delay, and τ_{ad} includes any additional system delays. It must be noted that the feeder link propagation latency τ_{feeder} contribution is two-fold because the estimations must be sent back to the ground station on the return link and the beamformed symbols to the satellite on the forward link.

Focusing on the on-board antenna illustrated in Figure 2, the array response of the UPA in the direction of the k -th UT (ϑ_k, φ_k) can be represented as the Kronecker product of the array responses of two uniform linear arrays (ULAs) aligned on the y -axis and the z -axis, respectively [21–24]. We first define the $1 \times N_H$ steering vector (SV) of the ULA along the y -axis as $\mathbf{a}_H(\vartheta_k, \varphi_k)$ and the $1 \times N_V$ SV of the ULA along the z -axis as follows $\mathbf{a}_V(\vartheta_k)$:

$$\mathbf{a}_H(\vartheta_k, \varphi_k) = [1, e^{jk_0 d_H \sin \vartheta_k \sin \varphi_k}, \dots, e^{jk_0 d_H (N_H - 1) \sin \vartheta_k \sin \varphi_k}] \quad (2)$$

$$\mathbf{a}_V(\vartheta_k) = [1, e^{jk_0 d_V \cos \vartheta_k}, \dots, e^{jk_0 d_V (N_V - 1) \cos \vartheta_k}] \quad (3)$$

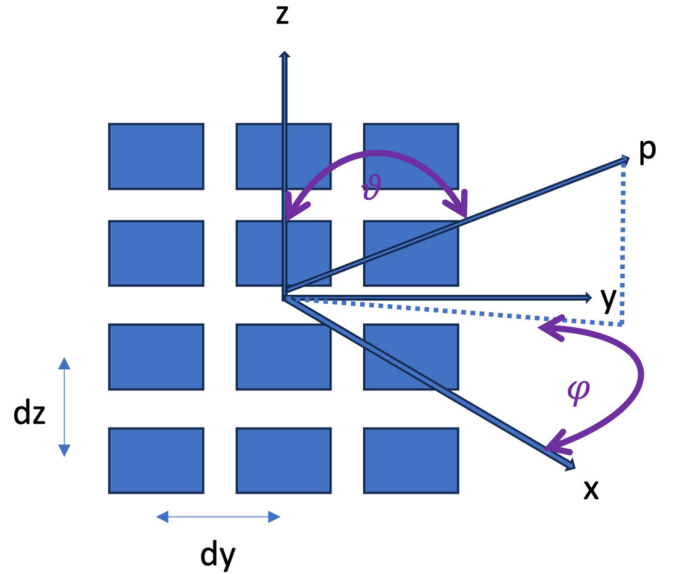


FIGURE 2 | Planar antenna array model [20].

In this context, additional information about the configuration and array response can be found in [25]. Under the assumption that the array is equipped with directional antenna elements, each characterized by the radiation pattern $g_E(\vartheta_k, \varphi_k)$, the $1 \times N$ SV of the UPA in the direction of the k -th UT can be expressed as follows:

$$\mathbf{a}(\vartheta_k, \varphi_k) = g_E(\vartheta_k, \varphi_k) \mathbf{a}_H(\vartheta_k, \varphi_k) \otimes \mathbf{a}_V(\vartheta_k) \quad (4)$$

where \otimes denotes the Kronecker product. Since we assume no availability of CSI, but only users' locations are available at the gNB, the FS channel vector between the N radiating elements of the UPA and the k -th UT can be inferred from the UT position by computing the slant range d_k and the UT direction (ϑ_k, φ_k) w.r.t. the UPA as follows:

$$\hat{\mathbf{h}}_k = G_k^{(rx)} \frac{\lambda}{4\pi d_k} \sqrt{\frac{1}{\kappa B T_k}} e^{-j \frac{2\pi}{\lambda} d_k} \mathbf{a}(\vartheta_k, \varphi_k) \quad (5)$$

where $G_k^{(rx)}$ is the maximum reception gain of the k -th UT's antenna, which is assumed to be a VSAT based on the 3GPP model reported in [26], pointed towards the satellite. By collecting all K channel vectors, we form the $K \times N$ complex system-level channel matrix, denoted as $\hat{\mathbf{H}}$. This matrix is structured as follows:

$$\hat{\mathbf{H}} = [\hat{\mathbf{h}}_1^T, \hat{\mathbf{h}}_2^T, \dots, \hat{\mathbf{h}}_K^T]^T \quad (6)$$

in which each row, specifically the k -th row, corresponds to the channel vector associated with the k -th user. Similarly, each column, particularly the n -th column, consists of the channel coefficients that relate the n -th feed to all K UTs. By looking at (5), $\hat{\mathbf{h}}_k$ and, consequently, $\hat{\mathbf{H}}$ are based on deterministic components and do not take into account the statistical additional losses L_k experienced by the k -th UT, computed as follows:

$$L_k = L_{sha,k} + L_{atm,k} + L_{sci,k} \quad (7)$$

where $L_{sha,k}$ denotes the attenuation due to log-normal shadowing, $L_{atm,k}$ the atmospheric attenuation, and $L_{sci,k}$ the attenuation due to the scintillation. Hence, the actual FS channel vector encountered during propagation can be written as follows:

$$\mathbf{h}_k = G_k^{(rx)} \frac{\lambda}{4\pi d_k} \sqrt{\frac{L_k}{\kappa BT}} e^{-j\frac{2\pi}{\lambda} d_k} \mathbf{a}(\theta_k, \varphi_k) \quad (8)$$

2.1 | Joint User Scheduling and Beamforming Setup

Given the set of all users that need to be scheduled, denoted with $\mathcal{U} = \{U_1, U_2, \dots, U_K\}$, the RRM algorithm has the task of allocating users to one or more clusters/groups $\{\mathcal{C}_1, \mathcal{C}_2, \dots, \mathcal{C}_P\}$, where $\mathcal{C}_p \subseteq \mathcal{U}$. To preserve fairness, we ensure that all users are allocated to at least one cluster, *i.e.*, $\mathcal{C}_1 \cup \mathcal{C}_2 \cup \dots \cup \mathcal{C}_P = \mathcal{U}$. Furthermore, we assume that the scheduling frame is composed by $T_{tot} = \sum_{p=1}^P K_p \geq K$ time slots, where K_p represents the cardinality of cluster \mathcal{C}_p , that is, $K_p = |\mathcal{C}_p|$. For each time slot, the RRM selects a cluster of users \mathcal{C}_p to be scheduled, resulting in a complex $K_p \times N$ scheduled channel matrix $\hat{\mathbf{H}}_p = \mathcal{F}(\hat{\mathbf{H}})$, where $\mathcal{F}(\cdot)$ represents the RRM scheduling function. Clearly, $\hat{\mathbf{H}}_p \subseteq \hat{\mathbf{H}}$. Then, the selected beamforming algorithm generates the corresponding complex $N \times K_p$ beamforming matrix $\mathbf{W}_p = [\mathbf{w}_1^{(p)}, \mathbf{w}_2^{(p)}, \dots, \mathbf{w}_{K_p}^{(p)}]$, where $\mathbf{w}_k^{(p)}$ represents the $N \times 1$ beamformer for the k -th user in the p -th cluster. Given the scheduled user unit-variance symbols vector $\mathbf{s}_p = [s_1, s_2, \dots, s_{K_p}]^T$, the matrix \mathbf{W}_p projects it onto the N -dimensional antenna FS, resulting in the generation of a beam for each user direction. The signal received by the k -th user in the p -th cluster can be expressed as follows:

$$y_k^{(p)} = \mathbf{h}_k \mathbf{w}_k^{(p)} s_k + \sum_{\substack{i=1 \\ i \neq k}}^{K_p} \mathbf{h}_k \mathbf{w}_i^{(p)} s_i + z_k^{(p)} \quad (9)$$

where $z_k^{(p)}$ is as a circularly symmetric Gaussian random variable with zero mean and unit variance representing additive white Gaussian noise (AWGN). Notice that \mathbf{h}_k here represents the actual channel encountered on the k -th link during propagation and it is, in general, mismatched with $\hat{\mathbf{h}}_k$ (and, thus, with $\mathbf{w}_k^{(p)}$). By collecting the signals received by all users within the same cluster, the resulting K_p -dimensional vector can be obtained as follows:

$$\mathbf{y}_p = \mathbf{H}_p \mathbf{W}_p \mathbf{s}_p + \mathbf{z}_p \quad (10)$$

The SINR for the k -th user in cluster p can be evaluated as follows:

$$\text{SINR}_k^{(p)} = \frac{\|\mathbf{h}_k \mathbf{w}_k^{(p)}\|^2}{1 + \sum_{\substack{i=1 \\ i \neq k}}^{K_p} \|\mathbf{h}_k \mathbf{w}_i^{(p)}\|^2} \quad (11)$$

To establish a fair-proportional scheduler, we allocate to each cluster a number of time slots T_p equal to its cardinality, that

is, $T_p = K_p$. Hence, the per-user achievable capacity for user k in cluster p can be computed as follows:

$$C_k = B \sum_{\substack{p \text{ s.t.} \\ U_k \in \mathcal{C}_p}} \gamma_p \log_2 \left(1 + \text{SINR}_k^{(p)} \right) \quad (12)$$

with γ_p denoting the weight for cluster p , which takes into account T_p as follows:

$$\gamma_p = \frac{K_p}{\sum_{p=1}^P K_p} = \frac{T_p}{T_{tot}} \quad (13)$$

In order to obtain the beamforming matrix \mathbf{W}_p , LB-MMSE beamformer is implemented. The algorithm resorts to the inferred channel matrix $\hat{\mathbf{H}}_p$ estimated at time t_0 . The resulting beamforming matrix is computed as follows:

$$\mathbf{W}_p = \hat{\mathbf{H}}_p^H (\hat{\mathbf{H}}_p \hat{\mathbf{H}}_p^H + \alpha \mathbf{I}_{K_p})^{-1} \quad (14)$$

where \mathbf{I}_{K_p} represents the $K_p \times K_p$ identity matrix and α is a regularization factor. Among the values proposed in the literature, we opted for the one specified in [27], where $\alpha = N/P_t$. It must be noted that, due to the rapid movement of LEO satellites, the latency Δt introduces a mismatch between the computed beamforming matrix and the actual propagation channel at transmission time \mathbf{H}_p .

2.2 | Power Normalizations

The Frobenius norm of the LB-MMSE beamforming matrix represents the satellite's total transmitted power. However, power normalization techniques must be employed to ensure that such value is bounded by on-board power restrictions [28]. The two power normalizations considered for this work are as follows:

- Sum-power constraint (SPC): This power normalization maintains orthogonality between beamforming matrix columns and ensures that the total power allotted by the matrix equals P_t without considering per-element power restrictions. This effect could lead to some high power amplifiers being driven close to their saturation regime, causing performance degradation due to the introduction of nonlinear effects.

$$\tilde{\mathbf{W}}_t^{(\text{SPC})} = \frac{\sqrt{P_{tot}} \mathbf{W}_t}{\sqrt{\text{tr}(\mathbf{W}_t \mathbf{W}_t^H)}} \quad (15)$$

- Maximum power constraint (MPC): This power normalization ensures that the power per feed is upper bounded, maintaining orthogonality. However, to accomplish this, the beamforming matrix is uniformly scaled with the most stringent power constraint, leading to part of the available on-board power being not utilized.

$$\bar{\mathbf{W}}_t^{(\text{MPC})} = \frac{\sqrt{P_{tot}} \mathbf{W}_t}{\sqrt{N \max_j [\mathbf{W}_t \mathbf{W}_t^H]_{jj}}} \quad (16)$$

3 | User Scheduling Algorithms

This section describes the schedulers that have been evaluated in this work. Two categories of algorithms can be identified: graph-based and non-graph-based schedulers.

3.1 | Graph-Based Schedulers

Let $\mathcal{G} = (\mathcal{V}, \mathcal{E})$ represent an undirected and unweighted graph, where \mathcal{V} is the set of vertices and \mathcal{E} is the set of edges. A clique \mathcal{Q} in graph \mathcal{G} is a subset of the vertices where every pair of distinct vertices is adjacent, that is, \mathcal{Q} forms a complete subgraph. In the LEO-based NTN MIMO scenario, the set of vertices \mathcal{V} is equivalent to the set of users \mathcal{U} , and the edge set is formed using a dissimilarity measure.

1. CSI-based IMCS (C-IMCS): If CSI is available at scheduling phase and therefore channel vectors \mathbf{h}_k can be obtained according to (8), the channel CoC [7] can be adopted as a dissimilarity measure, expressed as follows:

$$[\Psi]_{ij} = \frac{|\mathbf{h}_i \mathbf{h}_j^H|}{\|\mathbf{h}_i\| \|\mathbf{h}_j\|} \quad (17)$$

where $[\Psi]_{ij} \in [0, 1]$ measures the level of correlation between the estimated channel vector of users i and j . The set of edges \mathcal{E} of the \mathcal{G} graph is then completely determined by the adjacency matrix \mathbf{A} , which entries are defined as follows:

$$[\mathbf{A}]_{ij} = \begin{cases} 1, & \text{if } [\Psi]_{ij} \leq \delta_C \\ 0, & \text{if } [\Psi]_{ij} > \delta_C \end{cases} \quad (18)$$

where δ_C is a well-designed threshold. If $[\mathbf{A}]_{ij}$ is equal to 0, \mathbf{h}_i and \mathbf{h}_j are too similar to each other and the corresponding vertices have no edge between them. On the opposite, if $[\mathbf{A}]_{ij}$ is equal to 1, \mathbf{h}_i and \mathbf{h}_j are considered to be orthogonal enough for the corresponding users to be potentially assigned to the same cluster.

2. Distance-based IMCS (D-IMCS): When only users' positions are known at the scheduling phase, the great circle distance can be employed as a dissimilarity measure. This metric can be calculated by using the haversine formula, which takes into account the users' latitude ϕ_k and longitude λ_k as follows:

$$[\Gamma]_{ij} = 2 \arcsin \left(\sqrt{\sin^2 \left(\frac{\phi_j - \phi_i}{2} \right) + \cos \phi_i \cdot \cos \phi_j \cdot \sin^2 \left(\frac{\lambda_j - \lambda_i}{2} \right)} \right) \quad (19)$$

Using the inter-user distance as an inverse proxy for the CoC (i.e., it is assumed that $[\Psi]_{ij}$ increases as $[\Gamma]_{ij}$ decreases), we define the adjacency matrix \mathbf{A} as follows:

$$[\mathbf{A}]_{ij} = \begin{cases} 1, & \text{if } [\Gamma]_{ij} \geq \delta_D \\ 0, & \text{if } [\Gamma]_{ij} < \delta_D \end{cases} \quad (20)$$

where as in C-IMCS, δ_D is a well-optimized threshold. If $[\mathbf{A}]_{ij}$ is equal to 1, U_i and U_j are considered to be spatially separable using LB-MMSE digital beamforming, allowing them to belong to the same cluster. On the opposite, if $[\mathbf{A}]_{ij}$ equals 0, the great circle distance between the pair of users is too small for the users to be co-scheduled.

Both thresholds establish a limit to the clique size and, consequently, to the number of users that LB-MMSE beamforming inside a cluster may efficiently multiplex in the space domain; hence, their value must be optimized to maximize the system performance. A clique \mathcal{Q} of a graph \mathcal{G} is said to be maximal if it cannot be extended by including one more adjacent vertex, while a clique \mathcal{Q}_{\max} is said to be maximum if there does not exist any other clique with more vertices, that is, \mathcal{Q}_{\max} includes the largest possible number of vertices. Clearly, a maximum clique is also maximal, while the converse does not hold—Figure 3 illustrates the maximum clique \mathcal{Q}_{\max} of a graph \mathcal{G} made of 10 vertices. Using this concept, the graph-based user scheduling techniques employ a greedy iterative procedure to form the clusters $\{\mathcal{C}_1, \mathcal{C}_2, \dots, \mathcal{C}_P\}$, aiming at minimizing the number of clusters P . In particular, the two algorithms iteratively search and remove the maximum clique from \mathcal{G} , finding at each step the p -th group of scheduled users \mathcal{C}_p . Among the algorithm that tackle the maximum clique problem, for example, [29, 30], we implement at each iteration MaxCliqueDyn [31], a branch and bound algorithm that employs graph coloring-based sorting strategies and dynamic bounds to efficiently solve the maximum clique problem. MaxCliqueDyn can be considered an extension of the MCQ algorithm [32] with the inclusion of dynamically varying bounds. The pseudo-code for both C-IMCS and D-IMCS is reported in Algorithm 1. As previously reported, the difference between the two schedulers lies in the computation of the adjacency matrix \mathbf{A} , that is, C-IMCS uses (17) and D-IMCS uses (19).

3.2 | Non-Graph-Based Schedulers

- CSI-based MADOC (C-MADOC): The algorithm presented in [14] is based on a hybrid scheduling algorithm adopted from [7]. Originally developed to support satellite-based

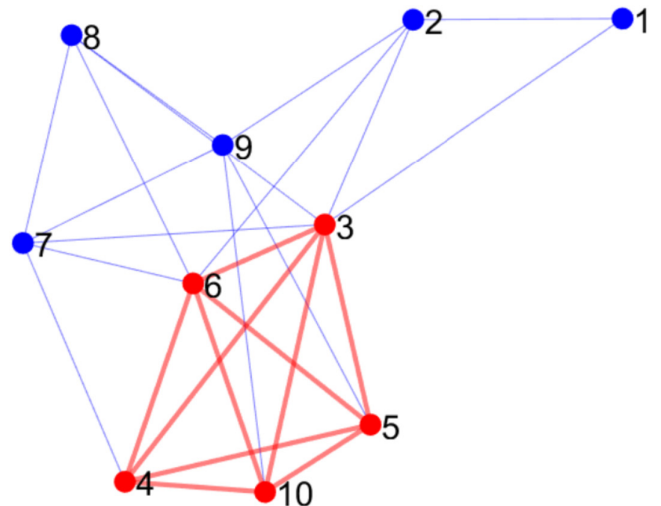


FIGURE 3 | Example graph with $\mathcal{U} = \{U_1, \dots, U_{10}\}$. The maximum clique \mathcal{Q}_{\max} is highlighted in red.

Algorithm 1 Iterative maximum clique scheduling algorithm**Input:**

Set of all users to be scheduled $\mathcal{U} = \{U_1, U_2, \dots, U_K\}$
 Adjacency matrix A

Output:

Cluster sets C_p
 Cluster weights γ_p for $p = 1, \dots, P$

```

1: Generate graph  $\mathcal{G}(\mathcal{U}, \mathcal{E})$ , with vertex set  $\mathcal{U}$  and edge set  $\mathcal{E}$ , where
    $\{U_i, U_j\} \in \mathcal{E}$  if  $[A]_{ij} = 1$ 
2: Initialize  $p = 1$ 
3:  $\mathcal{R} \leftarrow \mathcal{U}$ 
4: while  $\mathcal{R} \neq \emptyset$  do
5:    $Q_{\max} = \text{MaxCliqueDyn}(\mathcal{G})$ 
6:    $C_p \leftarrow Q_{\max}$ 
7:    $K_p \leftarrow |C_p|$ 
8:   for all  $U_i \in Q_{\max}$  do
9:     for all  $U_j \in \mathcal{R}$  do
10:       $\mathcal{E} = \mathcal{E} - \{U_i, U_j\}$ 
11:    end for
12:  end for
13:   $\mathcal{R} \leftarrow \mathcal{R} - Q_{\max}$ 
14:   $p \leftarrow p + 1$ 
15: end while
16: for  $p:=1$  to  $P$  do
17:    $\gamma_p \leftarrow \frac{K_p}{\sum_{p=1}^P K_p}$ 
18: end for

```

video-on-demand (VOD) applications with GEO satellites, C-MADOC employs the channel CoC computed from (17) as dissimilarity measure to create spatially compatible user groups. In particular, a group policy based on a threshold ϵ_C is used to create the so-called ϵ_C -orthogonal user groups; that is, for each user pair (U_i, U_j) in the same group, $[\Psi]_{ij} \leq \epsilon_C$ holds true. This ensures that a minimum level of orthogonality between user channels within each group is maintained. As for IMCS, the threshold value requires to be optimized. The algorithm minimizes the number of groups and ensures fairness so that the achieved data rates are homogeneous both inter-clusters and intra-cluster.

- Distance-based MADOC (D-MADOC): Instead of evaluating the spatial compatibility of users based on the channel CoC, we propose a variant of C-MADOC that considers the great circle distance matrix as grouping indicator based on (19). The D-MADOC algorithm only requires the users' positions in order to compute their slant ranges d_k and their inter-user distances $[\Gamma]_{ij}$. As illustrated in Algorithm 2, the procedure first identifies the minimum number of required clusters. In the original C-MADOC, the P users with the largest channel vector norm are selected to be the first user of each cluster; instead, we select the P users with the shortest slant range. In the main part of the algorithm, for every selected user $\{v\}$, the cluster \mathcal{C}_s is selected such that the inter-user distances between $\{v\}$ and all other users belonging to cluster \mathcal{C}_s are

Algorithm 2 Distance-based MADOC algorithm**Input:**

Set of all users to be scheduled $\mathcal{U} = \{U_1, U_2, \dots, U_K\}$
 Total number of feeds N
 Vector of users' slant ranges $\mathbf{d} = [d_1, d_2, \dots, d_K]$
 Users' great circle distance matrix Γ

Output:

Cluster sets C_p
 Cluster weights γ_p for $p = 1, \dots, P$

```

1:  $K = |\mathcal{U}|$ 
2:  $\mathcal{R} \leftarrow \mathcal{U}$ 
3:  $P = \lceil K/N \rceil$ 
4: Initialize  $C_1 = C_2 = \dots = C_P = \emptyset$ 
5: for  $p:=1$  to  $P$  do
6:    $v = \arg \min_{U_j \in \mathcal{R}} d_j$ 
7:    $C_p \leftarrow \{v\}$ 
8:    $\mathcal{R} \leftarrow \mathcal{R} - \{v\}$ 
9: end for
10: while  $\mathcal{R} \neq \emptyset$  do
11:    $v = \arg \min_{U_j \in \mathcal{R}} d_j$ 
12:    $s = \arg \max_{1 \leq p \leq P} \left( \min_{U_j \in C_p} [\Gamma]_{vj} \right)$ 
13:   if  $\min_{U_j \in C_p} [\Gamma]_{vj} > \epsilon_D$  then
14:      $C_s \leftarrow C_s \cup \{v\}$ 
15:   else
16:      $P = P + 1$ 
17:      $C_p \leftarrow \{v\}$ 
18:   end if
19:    $\mathcal{R} \leftarrow \mathcal{R} - \{v\}$ 
20:    $p \leftarrow p + 1$ 
21: end while
22: for  $p:=1$  to  $P$  do
23:    $K_p \leftarrow |C_p|$ 
24:    $\gamma_p \leftarrow \frac{K_p}{\sum_{p=1}^P K_p}$ 
25: end for

```

as high as possible: If all inter-user distances in $\mathcal{C}_s \cup \{v\}$ are above a certain threshold ϵ_D , user $\{v\}$ is added into cluster \mathcal{C}_s ; otherwise, a new cluster is created. Finally, user $\{v\}$ is removed from the user set \mathcal{U} and the procedure is repeated until there are no more users to be scheduled.

4 | Simulations and Results

This section presents the outcomes of extensive numerical assessments with parameters specified in Table 2. The analysis was carried out in the MATLAB environment employing Monte Carlo simulations. All the simulation parameters are based on [26, 33]. The key considerations are as follows:

- Standalone LEO satellite (600 km from Earth).
- UPA composed of 32×32 feeds.
- User density set to 0.05 users/km^2 .

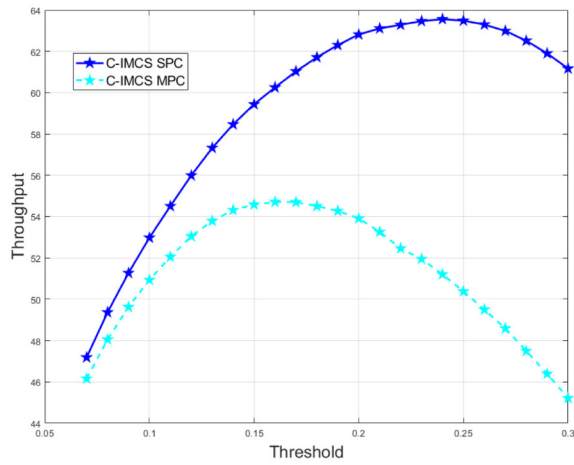
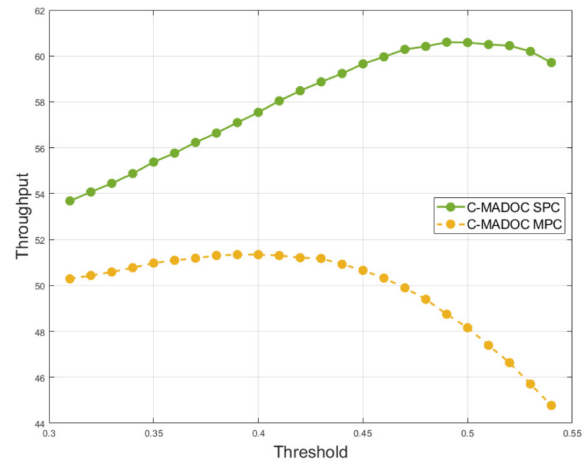
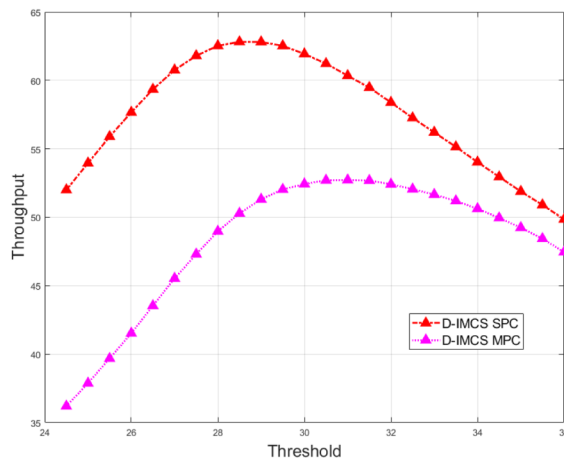
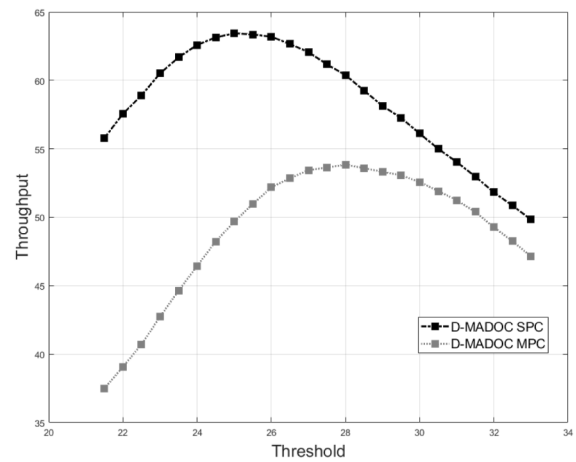
TABLE 2 | Simulation parameters.

Parameter	Value
Carrier frequency	20 GHz
System band	Ka (400 MHz)
Beamforming space	Feed
Receiver type	VSAT
Receiver antenna gain	39.7 dBi
Noise figure	1.2 dB
Propagation scenario	Line of sight (LOS)
System scenario	Urban
Total on-board power density, $P_{t,dens}$	4 dBW/MHz
Number of tiers	5
User density	0.05 user/km ²
Number of feeders N	1024 (32 × 32 UPA)
Monte Carlo iterations	100

- Fixed VSATs.

We initially conduct a heuristic optimization by running extensive simulations to determine the threshold values for the presented schedulers, aiming at maximizing the average per-user throughput. For C-IMCS and D-IMCS, the graph thresholds δ_C and δ_D control the graph's density, affecting the size K_p of the largest clique at each iteration. Figure 4a demonstrates that the optimal threshold for C-IMCS, δ_C , is 0.24 and 0.16 with SPC and MPC, respectively. With C-MADOC, illustrated in Figure 4b, the threshold ϵ_C has optimal values equal to 0.49 for SPC and 0.39 for MPC. We consider both these algorithms as benchmarks for the evaluation of the distance-based schedulers.

Figure 5a,b reports the optimization curves for the thresholds of D-IMCS and D-MADOC, respectively. For the newly proposed schedulers, the D-IMCS threshold δ_D obtains optimal values of 28.5 and 31 km with SPC-LB-MMSE and MPC-LB-MMSE, while in D-MADOC, ϵ_D has optimal values 25 and 28 km. One can notice that, for both schedulers, the optimal threshold for MPC-LB-MMSE is larger than the one for SPC-LB-MMSE, an

**(a)** C-IMCS threshold δ_C .**(b)** C-MADOC threshold ϵ_C .**FIGURE 4** | Threshold optimization for CSI-based schedulers.**(a)** D-IMCS threshold δ_D .**(b)** D-MADOC threshold ϵ_D .**FIGURE 5** | Threshold optimization for distance-based schedulers.

opposite behavior with respect to the CSI-based schedulers. This is to be expected, as the CSI-based thresholds are inversely proportional to the degree of dissimilarity (i.e., a higher threshold value corresponds to higher channel co-linearity), while the distance-based thresholds are directly proportional to the degree

of dissimilarity (a higher threshold value corresponds to a larger distance and, hence, an increased orthogonality). This remark also justifies the opposite trend of the SPC-LB-MMSE and MPC-LB-MMSE optimization curves for CSI-based schedulers, where the performance gap between the two power normalizations increases with the threshold value and for the distance-based algorithms, where an increase in threshold value shrinks such gap.

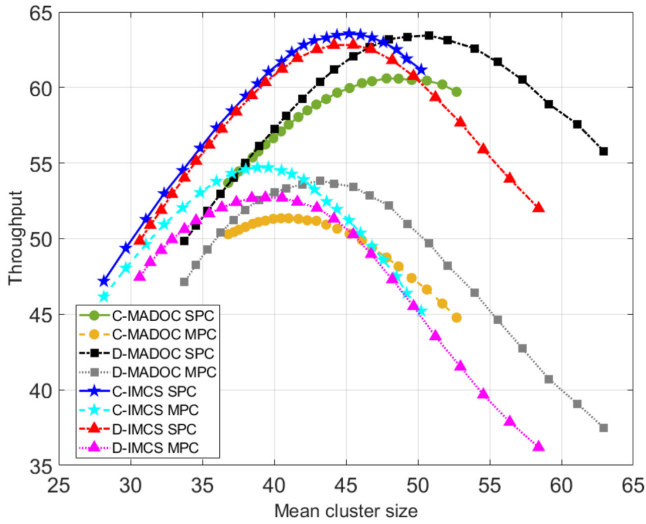


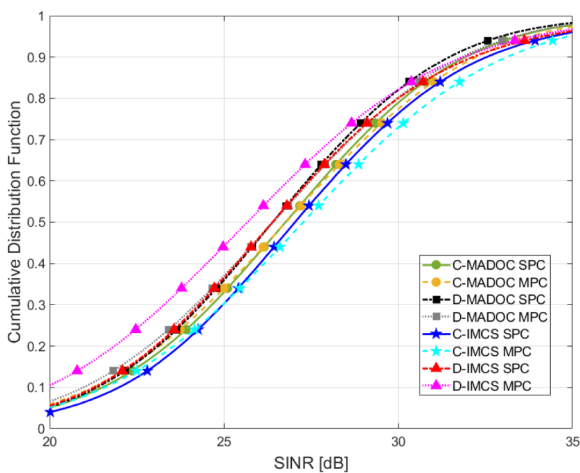
FIGURE 6 | Throughput vs. mean cluster size.

Figure 6 reports the achievable average throughput as a function of the mean cluster sizes for each scheduler and power normalization. The plot shows that D-MADOC tends to form better performing and larger clusters than its CSI-based counterpart, while C-IMCS is the best performing algorithm (also better than D-MADOC), slightly superior to its distance-based counterpart. It can also be noticed that the gap in performance between D-MADOC and C-MADOC is much larger than between C-IMCS and D-IMCS.

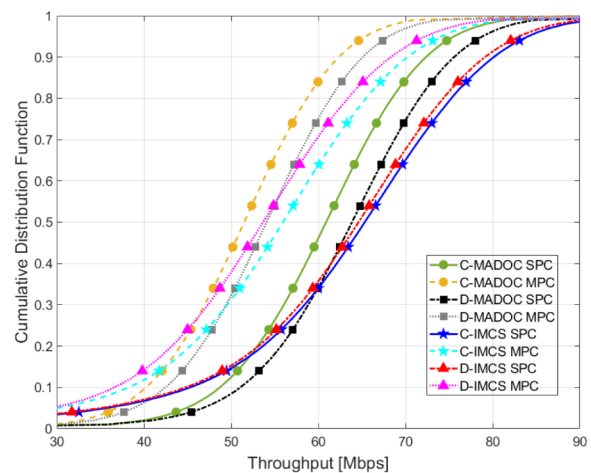
Table 3 presents a detailed overview of the optimal threshold values, mean cluster sizes, mean number of clusters, and average per-user throughput. All results are specified for the two considered power normalizations. The table shows that D-MADOC achieves an average per-user throughput of 63.44 and 53.84 Mbps with SPC and MPC power normalization, respectively. This corresponds to a performance increase of 2.84

TABLE 3 | Simulation results.

Parameters	Power normalization	C-IMCS	C-MADOC	D-IMCS	D-MADOC
Thresholds	SPC	0.24	0.49	28.5	25
$\delta_C, \epsilon_C, \delta_D, \epsilon_D$	MPC	0.16	0.39	31	28
Mean cluster size	SPC	44.37	46.81	46.74	52.07
	MPC	38.02	39.94	40.55	44.18
Mean number of clusters	SPC	63.06	59.63	62.66	56.18
	MPC	73.42	70.44	72.39	66.04
Average per-user throughput (Mbps)	SPC	63.56	60.60	62.82	63.44
	MPC	54.71	51.35	52.72	53.84

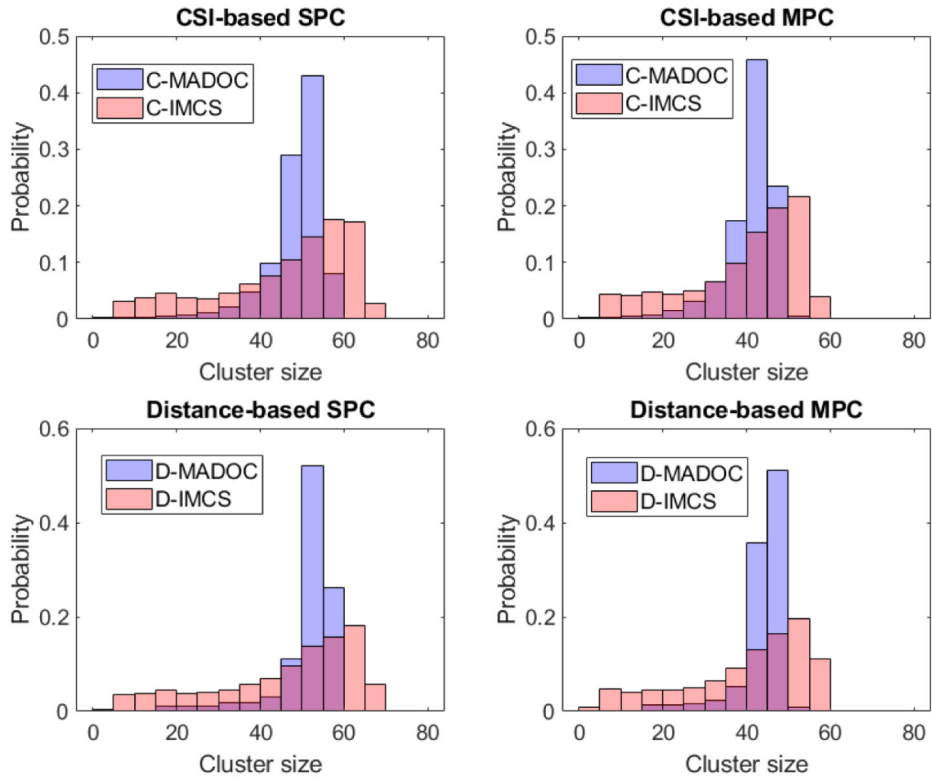


(a) CDF of the users' SINR [dB].

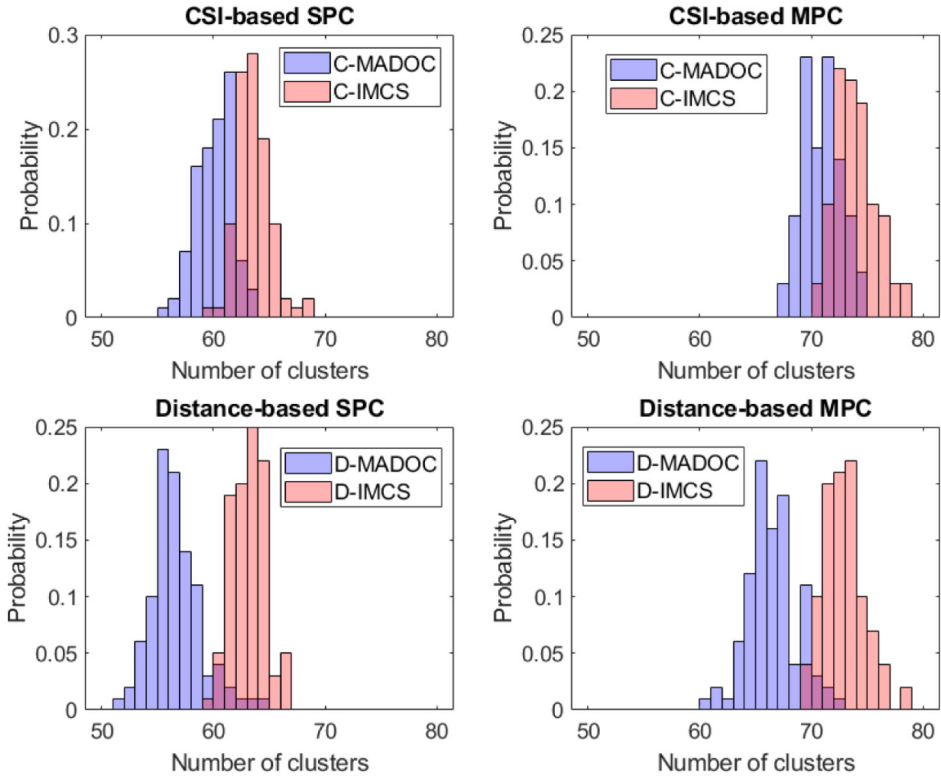


(b) CDF of the per-user throughput.

FIGURE 7 | CDFs of the users' SINR and the per-user throughput.



(a) Empirical probability distribution of the cluster size.



(b) Empirical probability distribution of the number of clusters.

FIGURE 8 | Empirical probability distribution of the cluster size and number of clusters for CSI-based and distance-based schedulers.

Mbps (4.69%) and 2.49 Mbps (4.85%) with respect to C-MADOC. However, the distance-based metric is not able to provide similar gains to the IMCS scheduler, leading to a throughput reduction of 740 kbps with SPC normalization and 1.99 Mbps with MPC normalization.

Figure 7a shows the cumulative distribution function (CDF) of the users' SINR for each scheduler and power normalization. Clearly, the implementation of the distance-based scheduling metric results in an overall lower SINR than what is achieved by the CSI-based counterpart, regardless of the scheduling approach and power normalization. However, recalling (12) and (13), the choice of the scheduler affects the throughput through not only the SINR but also the size of the created clusters. As reported in Table 3, the introduction of the distance-based metric consistently results in an increase in the mean cluster size. Hence, the user throughput requires a dedicated analysis.

Figure 7b reports the CDF of the user throughput. Starting from the non-graph-based scheduler, D-MADOC shows a performance improvement over C-MADOC, with the MPC-LB-MMSE beamformer achieving an increase of the median (i.e., 50th percentile) throughput by 2.56 Mbps with similar fairness. We report even better improvements when SPC-LB-MMSE is employed, with a performance gap of 2.97 Mbps. Clearly, the distance-based metric allows the algorithm to create larger clusters than the CSI-based counterpart, balancing the effect on the SINR observed in Figure 7a. On the other hand, the D-IMCS scheduler does not provide clear advantages over C-IMCS. In particular, with SPC normalization, the curves exhibit similar behavior, implying that a similar fairness is achieved, but the median user throughput incurs in a loss of 706 kbps. It is also interesting to notice that D-MADOC achieves the best throughput fairness w.r.t. C-MADOC and both graph-based schedulers, as demonstrated by lower 20 %-ile (D-MADOC 55.73 Mbps vs. C-IMCS 53.66 Mbps). Clearly, the distance-based metric can result in noticeable performance improvements, but this does not hold true for any scheduler it is applied to. Further studies may be carried on to determine whether such behavior is to be expected for any graph-based scheduler.

Finally, Figure 8 shows the empirical probability distribution by means of histograms of the cluster size (Figure 8a) and of the number of clusters (Figure 8b) for all considered schedulers and power normalizations. As far as the cluster size is concerned, MADOC schedulers show a narrower distribution with a peak in cluster size between 50 and 55 UTs for both C-MADOC and D-MADOC with SPC, while with MPC, the peak is in the range 40–45 UTs for C-MADOC and 45–50 UTs for D-MADOC, respectively. The graph-based schedulers show instead a more uniform empirical distribution. This behavior can be justified by the greedy nature of the IMCS algorithm: At the first iterations, when most of the users have yet to be scheduled, both C-IMCS and D-IMCS are able to produce larger clusters in size than MADOC (up to 75 UTs per cluster for SPC and 60 UTs for MPC); however, as the graph gets more and more pruned, the sizes of the cliques become smaller. Figure 8b shows the distribution of the number of clusters or equivalently, the number of time slots; it can be noticed that MADOC in general requires less time slots to accommodate all users w.r.t. the graph-based schedulers, with a clear reduction of time slots for D-MADOC

compared to C-MADOC. To summarize, given the performance results, the mean cluster size, and mean number of time slots for all techniques, MADOC can better exploit the available resources (less time slots), while IMCS has a better interference management within each cluster.

5 | Conclusion

In this work, we have provided an analysis and evaluation of graph- and non-graph-based schedulers for LEO-based NTN systems operating at Ka-band. We have established the concept of using the users' great circle distance as the basis for clustering and proposed it to be adopted as a dissimilarity measure, so that only the users' positions are required instead of their CSI. Within each cluster, we utilize location-based minimum mean square error beamforming to accomplish spatial multiplexing of the co-scheduled users. We have considered two different methods of power normalization for the beamforming matrix: sum power constraint and MPC. We have further conducted an extensive evaluation to identify the optimized threshold values which maximize the average per-user throughput for both distance-based schedulers: (a) a distance-based iterative graph-based scheduler based on the maximum clique approach and (b) a distance-based variant of the MADOC algorithm. We have further compared the results with the CSI-based versions of the graph-based scheduler and MADOC. The results of our investigation are presented in terms of per-user throughput and SINR and demonstrate that the distance-based grouping indicator can be quite effective in designing user scheduling algorithms.

Acknowledgments

This work was partially supported by the European Union under the Italian National Recovery and Resilience Plan (NRRP) of NextGenerationEU, partnership of "Telecommunications of the Future" (PE00000001 - program "RESTART"), and funded by the 6G-NTN project, which received funding from the Smart Networks and Services Joint Undertaking (SNS JU) under the European Union's Horizon Europe Research and Innovation Programme under grant agreement no. 101096479. The views expressed are those of the authors and do not necessarily represent the project. The Commission is not liable for any use that may be made of any of the information contained therein. Open access publishing facilitated by Consiglio Nazionale delle Ricerche, as part of the Wiley - CRUI-CARE agreement.

The work of Daniel Gaetano Riviello was partially supported by the European Union - NextGenerationEU - National Recovery and Resilience Plan (Piano Nazionale di Ripresa e Resilienza, PNRR) through the Project: "SoBigData.it - Strengthening the Italian RI for Social Mining and Big Data Analytics", under grant prot. IR0000013 - Avviso no. 3264 del 28/12/2021.

Conflicts of Interest

The authors declare no conflicts of interest.

References

1. G. Araniti, A. Iera, S. Pizzi, and F. Rinaldi, "Toward 6G Non-Terrestrial Networks," *IEEE Network* 36, no. 1 (2022): 113–120, <https://doi.org/10.1109/MNET.011.2100191>.

2. A. Guidotti, A. Vanelli-Coralli, M. El Jaafari, et al., "Role and Evolution of Non-Terrestrial Networks Toward 6G Systems," *IEEE Access* 12 (2024): 55945–55963, <https://doi.org/10.1109/ACCESS.2024.3389459>.
3. A. Di Mezza, A. Vanelli Coralli, A. Guidotti, T. Foggi, G. Colavolpe, and G. Montorsi, "5G4SPACE: Adaptation of 5G Radio Access Technology for Satcom", *2019 International Symposium on Advanced Electrical and Communication Technologies (ISAECT)*, Rome, Italy, 2019, pp. 1–3, <https://doi.org/10.1109/ISAECT47714.2019.9069675>.
4. E. Castaneda, A. Silva, A. Gameiro, and M. Kountouris, "An Overview on Resource Allocation Techniques for Multi-User MIMO Systems," *IEEE Communications Surveys & Tutorials* 19, no. 1 (2017): 239–284, <https://doi.org/10.1109/COMST.2016.2618870>.
5. A. Ugolini, Y. Zanetini, A. Piemontese, A. Vanelli-Coralli and G. Colavolpe, "Efficient Satellite Systems Based on Interference Management and Exploitation", *2016 50th Asilomar Conference on Signals, Systems and Computers*, Pacific Grove, CA, USA, 2016, pp. 492–496, <https://doi.org/10.1109/ACSSC.2016.7869088>.
6. A. Guidotti and A. Vanelli Coralli, "Clustering Strategies for Multicast Precoding in Multibeam Satellite Systems," *International Journal of Satellite Communications and Networking* 38, no. 2 (2020): 85104, <https://doi.org/10.1002/sat.1312>.
7. X. Yi and E. K. S. Au, "User Scheduling for Heterogeneous Multiuser MIMO Systems: A Subspace Viewpoint," *IEEE Transactions on Vehicular Technology* 60, no. 8 (2011): 4004–4013, <https://doi.org/10.1109/TVT.2011.2165976>.
8. M. Vzquez and A. I. Prez-Neira, "Spectral Clustering for Beam-Free Satellite Communications", *2018 IEEE Global Conference on Signal and Information Processing (GlobalSIP)*, Anaheim, CA, USA, 2018, pp. 1030–1034, <https://doi.org/10.1109/GlobalSIP.2018.8646351>.
9. D. Christopoulos, S. Chatzinotas, and B. Ottersten, "Multicast Multigroup Precoding and User Scheduling for Frame-Based Satellite Communications," *IEEE Transactions on Wireless Communications* 14, no. 9 (2015): 4695–4707, <https://doi.org/10.1109/TWC.2015.2424961>.
10. W. Wang, A. Liu, Q. Zhang, L. You, X. Gao, and G. Zheng, "Robust Multigroup Multicast Transmission for Frame-Based Multi-Beam Satellite Systems," *IEEE Access* 6 (2018): 46074–46083, <https://doi.org/10.1109/ACCESS.2018.2865998>.
11. P. J. Honnaiah, E. Lagunas, D. Spano, N. Maturo and S. Chatzinotas, "Demand-Based Scheduling for Precoded Multibeam High-Throughput Satellite Systems", *2021 IEEE Wireless Communications and Networking Conference (WCNC)*, Nanjing, China, 2021, pp. 1–6, <https://doi.org/10.1109/WCNC49053.2021.9417300>.
12. J. P. Gonzalez-Coma, F. J. Lopez-Martinez, and L. Castedo, "Low-Complexity Distance-Based Scheduling for Multi-User XL-MIMO Systems," *IEEE Wireless Communications Letters* 10, no. 11 (2021): 2407–2411, <https://doi.org/10.1109/LWC.2021.3101940>.
13. H. Chen and C. Qi, "User Grouping for Sum-Rate Maximization in Multiuser Multibeam Satellite Communications", *ICC 2019-2019 IEEE International Conference on Communications (ICC)*, Shanghai, China, 2019, pp. 1–6, <https://doi.org/10.1109/ICC.2019.8761875>.
14. K.-U. Storek and A. Knopp, "Fair User Grouping for Multibeam Satellites With MU-MIMO Precoding", *GLOBECOM 2017-2017 IEEE Global Communications Conference*, Singapore, 2017, pp. 1–7, <https://doi.org/10.1109/GLOCOM.2017.8255098>.
15. B. Ahmad, D. G. Riviello, B. De Filippo, A. Guidotti, and A. Vanelli Coralli, "Analysis of Graph-Based User Scheduling for Ka-Band LEO NTN Systems", *28th Ka and Broadband Communications Conference (Ka) and the 40th International Communications Satellite Systems Conference (ICSSC)*, Bradford, United Kingdom, 2023. [Online]. Available: https://proceedings.kaconf.com/papers/2023/ka9_2.pdf.
16. D. G. Riviello, B. Ahmad, A. Guidotti, and A. Vanelli Coralli, "Joint Graph-Based User Scheduling and Beamforming in LEO-MIMO Satellite Communication Systems", *2022 11th Advanced Satellite Multimedia Systems Conference and the 17th Signal Processing for Space Communications Workshop (ASMS/SPSC)*, Graz, Austria, 2022, pp. 1–8, <https://doi.org/10.1109/ASMS/SPSC55670.2022.9914723>.
17. B. Ahmad, D. G. Riviello, A. Guidotti, and A. Vanelli Coralli, "Graph-Based User Scheduling Algorithms for LEO-MIMO Non-Terrestrial Networks", *2023 Joint European Conference on Networks and Communications & 6G Summit (EuCNC/6G Summit)*, Gothenburg, Sweden, 2023, pp. 270–275, <https://doi.org/10.1109/EuCNC/6GSummit58263.2023.10188287>.
18. B. Ahmad, D. G. Riviello, A. Guidotti, and A. Vanelli Coralli, "Improved Graph-Based User Scheduling for Sum-Rate Maximization in LEO-NTN Systems", *2023 IEEE International Conference on Acoustics, Speech, and Signal Processing Workshops (ICASSPW)*, Rhodes Island, Greece, 2023, pp. 1–5, <https://doi.org/10.1109/ICASSPW59220.2023.10193499>.
19. B. De Filippo, B. Ahmad, D. G. Riviello, A. Guidotti, and A. Vanelli-Coralli, "Non-Uniform User Distribution in Non-Terrestrial Networks With Application to User Scheduling", *2024 IEEE International Mediterranean Conference on Communications and Networking (MeditCom)*, Madrid, Spain, 2024, pp. 441–446, <https://doi.org/10.1109/MeditCom61057.2024.10621409>.
20. D. G. Riviello, B. De Filippo, B. Ahmad, A. Guidotti, and A. Vanelli-Coralli, "Location-based User Scheduling Through Graph Coloring for Cell-Free MIMO NTN Systems," in *2024 Joint European Conference on Networks and Communications & 6G Summit (EuCNC/6G Summit)* (Antwerp, Belgium: 2024): 652–657, <https://doi.org/10.1109/EuCNC/6GSummit60053.2024.10597125>.
21. H. L. Van, *Trees, Optimum Array Processing: Part IV of Detection, Estimation, and Modulation Theory* (John Wiley & Sons, 2002), <https://doi.org/10.1002/0471221104>.
22. G. Alfano, C.-F. Chiasserini, A. Nordio, and D. G. Riviello, "A Random Matrix Model for mmWave MIMO Systems," *Acta Physica Polonica B* 51, no. 7 (2020): 1627–1640, <https://doi.org/10.5506/APhysPolB.51.1627>.
23. D. G. Riviello, R. Tuninato, and R. Garello, "Multi-Layer Multi-User MIMO With Cylindrical Arrays Under 3GPP 3D Channel Model for B5G/6G Networks," *IEEE Access* 12 (2024): 145753–145767, <https://doi.org/10.1109/ACCESS.2024.3472489>.
24. D. G. Riviello and R. Garello, "Implementation of 5G Beamforming Techniques on Cylindrical Arrays", *2019 IEEE-APS Topical Conference on Antennas and Propagation in Wireless Communications (APWC)*, Granada, Spain, 2019, pp. 413–418, <https://doi.org/10.1109/APWC.2019.8870441>.
25. ITU-R Radiocommunication Sector of ITU, "Modelling and Simulation of IMT Networks and Systems for Use in Sharing and Compatibility Studies (M.2101-0)", Feb. 2017.
26. 3GPP, "TR 38.821 - Solutions for NR to Support Non-Terrestrial Networks (NTN)", May 2021.
27. A. Guidotti and A. Vanelli Coralli, "Geographical Scheduling for Multicast Precoding in Multi-Beam Satellite Systems", *9th Advanced Satellite Multimedia Systems Conference and the 15th Signal Processing for Space Communications Workshop (ASMS/SPSC)*, Berlin, Germany, 2018, pp. 1–8, <https://doi.org/10.1109/ASMS-SPSC.2018.8510728>.
28. I. Ahmad, K. D. Nguyen, N. Letzepis, G. Lechner, and V. Jorroughi, "Zero-Forcing Precoding With Partial CSI in Multibeam High Throughput Satellite Systems," *IEEE Transactions on Vehicular Technology* 70, no. 2 (2021): 1410–1420, <https://doi.org/10.1109/TVT.2021.3052225>.

29. P. Prosser, "Exact Algorithms for Maximum Clique: A Computational Study," *Algorithms* 5, no. 4 (2012): 545–587, <https://doi.org/10.3390/a5040545>.
30. A. Douik, H. Dahrouj, T. Y. Al-Naffouri, and M.-S. Alouini, "A Tutorial on Clique Problems in Communications and Signal Processing," *Proceedings of the IEEE* 108, no. 4 (2020): 583–608, <https://doi.org/10.1109/JPROC.2020.2977595>.
31. J. Konc and D. Janezic, "An Improved Branch and Bound Algorithm for the Maximum Clique Problem," *MATCH Communications in Mathematical and in Computer Chemistry* 58, no. 3 (2007): 569590. [Online]. Available:., <http://www.insilab.org/articles/match2007.pdf>.
32. E. Tomita and T. Seki, "An Efficient Branch-and-Bound Algorithm for Finding a Maximum Clique," in *Discrete Mathematics and Theoretical Computer Science. DMTCS 2003. Lecture Notes in Computer Science*, vol. 2731 (Berlin, Heidelberg: Springer, 2003), https://doi.org/10.1007/3-540-45066-1_22.
33. 3GPP, "TR 38.811 - Study on New Radio (NR) to Support Non-Terrestrial Networks (Release 15)", Sep. 2020.